J. Fluid Mech. (1983), *vol.* 126, *pp.* 545–567
Printed in Great Britain

Steady and oscillatory thermocapillary convection in liquid columns with free cylindrical surface

By F. PREISSER, D. SCHWABE AND A. SCHARMANN
I. Physikalisches Institut, Justus-Liebig-Universität, Heinrich-Buff-Ring 16, D-6300 Giessen, W. Germany

(Received 8 September 1981 and in revised form 30 June 1982)

In liquid columns (Prandtl number 8·9) with free cylindrical surface heated from above, strong thermocapillary convection (TC) has been observed. Stationary thermocapillary convection exists in the form of a single axially symmetric roll bound to the free surface. For aspect ratios $l/a < 1$ the radial extension of the roll equals the zone length. The stream velocities and the temperature distribution were measured.

The influence of buoyant forces due to horizontal temperature gradients in the experiments was also studied. Buoyant forces become obvious for a contaminated free surface and in bulk regions far from the cylinder surface.

The thermocapillary convection shows a transition to time-dependent oscillatory motion when a critical Marangoni number Ma_c is exceeded. A unique $Ma_c = 7 \times 10^3$ has been found for zones with lengths $l < 3{\cdot}5$ mm. The oscillatory state of thermocapillary convection has experimentally been proved to be a distortion of the laminar state in form of a wave travelling in the azimuthal direction. A unique non-dimensional wavenumber $\approx 2{\cdot}2$ (near Ma_c) of the distortion has been found. The non-dimensional frequency of the temperature oscillations is independent of zone size if the aspect ratio is held constant. However, the non-dimensional frequency of temperature oscillations increases linearly with the aspect ratio of the zone. This result is interpreted as a dependence of the phase velocity of the running disturbance on the aspect ratio.

1. Introduction

The presence of an unbalanced surface-tension gradient in the free surface between a liquid and a gaseous phase will influence the motion of these media. Since the surface tension depends significantly on temperature, temperature gradients along the surface drive a flow, because gradients of surface tension act like shear stress on the adjoining bulk fluids. If the surface-tension gradient is maintained by sources and sinks of heat, a perpetual surface flow is generated from regions of low surface tension to regions of higher surface tension or existing flows are continuously influenced. A lot of previous work has been concerned with Marangoni convection in thin films where the temperature gradient is applied *perpendicular to the free surface*. It is now known that thermally stimulated surface-tension gradients cause the hexagonal flow pattern (Bénard's original experiment) in liquid layers with free upper surface subjected to destabilizing density gradients. Experiments of Block (1956) and theoretical investigations of Scriven & Sternling (1964), Pearson (1958), Nield (1964) and Smith (1966) have confirmed the important role of Marangoni convection for cellular buoyant convection. In contrast, flows driven by a temperature gradient

aligned *parallel to the free surface*, which are called thermocapillary convection (TC), seem to have received less attention in hydrodynamics. However, continuous progress in the investigation of TC has been made in the theoretical works of Levich (1962), Birikh (1966) and Ostrach (1977) in two-dimensional configurations. These investigations have shown that, in contrast to Marangoni convection, TC sets in at any temperature gradient, however small it may be, and typically produces maximal flow speed in the free surface. Recent studies on TC have been triggered by the need in the materials-science field to elucidate the importance of TC in materials processing. Calculations by Chang & Wilcox (1976) and Clark & Wilcox (1980) demonstrated that TC dominates buoyant convection in cylindrical volumes up to 1 cm^3. Steady TC has been observed directly in small liquid volumes (radii up to 10 mm, lengths up to 7 mm) of medium and high Prandtl number by Schwabe *et al.* (1978), Schwabe, Scharmann & Preisser (1979), Chun & Wuest (1978), and Ostrach and co-workers (S. Ostrach 1981 private communication). Furthermore, the interest in TC in floating zones is stimulated by the finding that is shows a transition into a time-dependent flow state (Schwabe *et al.* 1978; Chun & Wuest 1979) above a certain vertical temperature gradient (Schwabe & Scharmann 1979).

The analysis of steady and time-dependent TC and its interactions with density-driven convection can be valuably applied to a large number of techniques in solid-state processing and physico-chemical engineering. Especially in crystal-growth methods of high technical importance, the existence of a free surface with a steep temperature gradient is inherent. Therefore TC can contribute to the mass and heat flows in these systems, as has been calculated by Langlois (1980, 1981) and has recently been proved experimentally by Schwabe & Scharmann (1981). A review on Marangoni effects in crystal growth melts by Schwabe (1981*a*) gives further details and references.

The relevance of time-dependent TC for crystal-growth processes is obvious, because it is well known that an unsteady flow in the liquid phase causes the quality of the growing crystal to deteriorate considerably.

The importance of surface-tension-gradient-driven flows in melting technologies under reduced gravity has been discussed in detail, since there are possibilities of experiments in spacecraft. As density-driven convection will be of negligible influence in a microgravity environment, Marangoni convection and TC will provide a means of powerful convective mixing in melts with free surface. The existence of Marangoni convection in the form of cellular flow has already been demonstrated aboard the Apollo space vehicle (Grodzka & Bannister 1975). Studies of the features of TC are needed to prepare planned crystal-growth experiments in Spacelab.

The present paper reports experimental data on laminar and time-dependent TC in floating zones of various lengths and diameters.

2. Parameters, experimental apparatus and technique

A zone is a cylindrical vertical column with radius a, height (= length) l, and aspect ratio $A = l/a$. For the description of results the origin of the cylindrical coordinates is placed in the centre of the bottom end face.

The dimensionless radial and axial coordinates are defined as $R = r/a$ and $Z = z/l$. ΔT is the applied temperature difference between the upper and lower solid boundary; $\theta = (T - T_{\text{lower}})/(T_{\text{upper}} - T_{\text{lower}}) = (T - T_{\text{lower}})/\Delta T$ is the non-dimensional temperature. As dimensionless number for TC in the zone the Marangoni number Ma is used:

$$Ma = \left|\frac{\partial \sigma}{\partial T}\right| \eta^{-1} \chi^{-1} \Delta T l, \tag{1}$$

where $\partial\sigma/\partial T$ is the temperature coefficient of surface tension, η the dynamic viscosity and χ the thermal diffusivity.

The experimental chamber is shown in figure 1 with some details not mentioned in the text. The chamber is axially symmetric except in the middle segment, which has four quartz windows. The upper and lower segments contain heating elements for applying different temperature gradients along the zone surface. Natural convection in the gas surrounding the zone and horizontal temperature gradients near the zone have been minimized. The graphite rods are made from graphite of highest thermal conductivity (λ(graphite) = $1{\cdot}70 \times 10^7$ erg s^{-1} cm^{-1} K^{-1}, type FE 534 from Schunk & Ebe) and are coated with pyrolytic graphite to prevent chemical reaction with the zone liquid and to reduce the wetting properties. The length of the zone can be varied continuously by movement of the upper heating element with a micrometer. To change the zone diameter, graphite rods with various diameters are screwed in the copper cylinders.

Melting point T_m	306·8	°C
Density ρ	1·903	g cm^{-3}
Coefficient of expansion $\partial\rho/\partial T$	$-3{\cdot}80 \times 10^{-4}$	K^{-1}
Surface tension σ	119·7	dyn cm^{-1}
Temperature coefficient of surface tension $\partial\sigma/\partial T$	$-5{\cdot}5 \times 10^{-2}$	dyn cm^{-1} K^{-1}
Dynamic viscosity η	$2{\cdot}82 \times 10^{-2}$	g s^{-1} cm^{-1}
Kinematic viscosity ν	$1{\cdot}48 \times 10^{-2}$	cm^2 s^{-1}
Thermal conductivity λ	$5{\cdot}71 \times 10^4$	erg s^{-1} cm^{-1} K^{-1}
Thermal diffusivity χ	$1{\cdot}67 \times 10^{-3}$	cm^2 s^{-1}
Specific heat c_p	$1{\cdot}80 \times 10^7$	erg g^{-1} K^{-1}
Prandtl number Pr	8·9	
Factor in Marangoni number $\lvert\partial\sigma/\partial T\rvert\eta^{-1}\chi^{-1}$	1168	cm^{-1} K^{-1}

TABLE 1. Physical properties of liquid $NaNO_3$ at 320 °C (obtained from linear interpolation of data given in Janz 1967; Landolt-Börnstein 1969, 1971; D'Ans-Lax 1964)

The zone liquid is molten $NaNO_3$. The relevant physical data are listed in table 1. $NaNO_3$ is chemically stable up to approximately 400 °C and the melt is fully transparent. The high-temperature coefficient of surface tension allows large Marangoni numbers. The medium Prandtl number is in the range of some crystal-growth melts of high technical importance and, by the high working temperature of the fluid, the thermal boundary conditions of melts are better simulated than with the usual oils. The experiments have shown the free surface to be insensitive to normal contamination such as dust (except oil). The contact angle between pyrolytically coated graphite and liquid $NaNO_3$ is approximately 90°; therefore zones with lengths under 4 mm have an ideal cylindrical shape. Filling of a zone was made with a heated quartz syringe (pyrolytically coated with graphite).

PID-controllers provided temperature control of the heating elements with an accuracy of $\pm 0{\cdot}1$ K. The absolute temperature of each graphite rod end face is measured within $\pm 0{\cdot}5$ K by a thin NiCr–Ni thermocouple that is located 0·5 mm in front of the endface in a blind hole.

Measurements are started after a thermalization time of 1–2 h. For changes of the temperature difference in the range of less than 10 K the thermalization time was 5–10 min, which is long compared with the characteristic thermal diffusion time

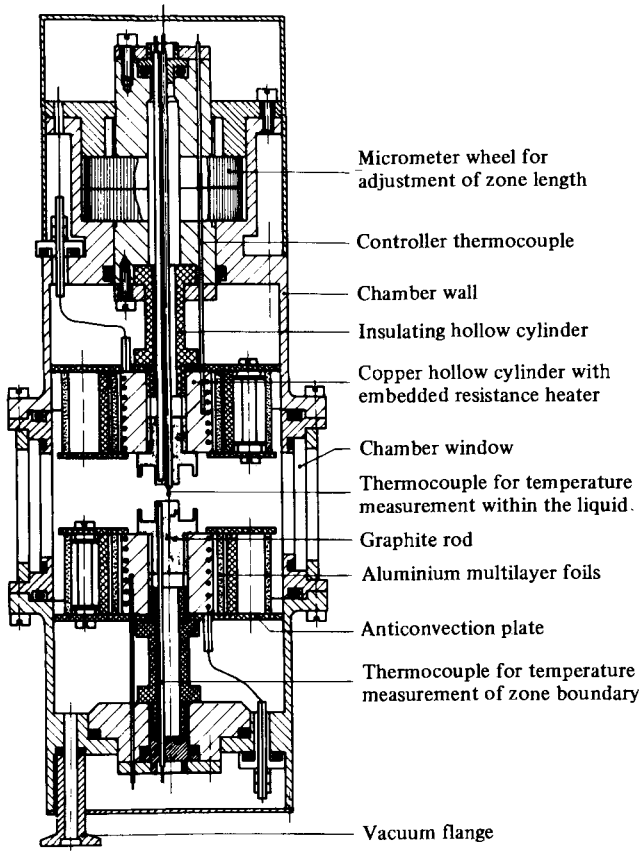

(a)

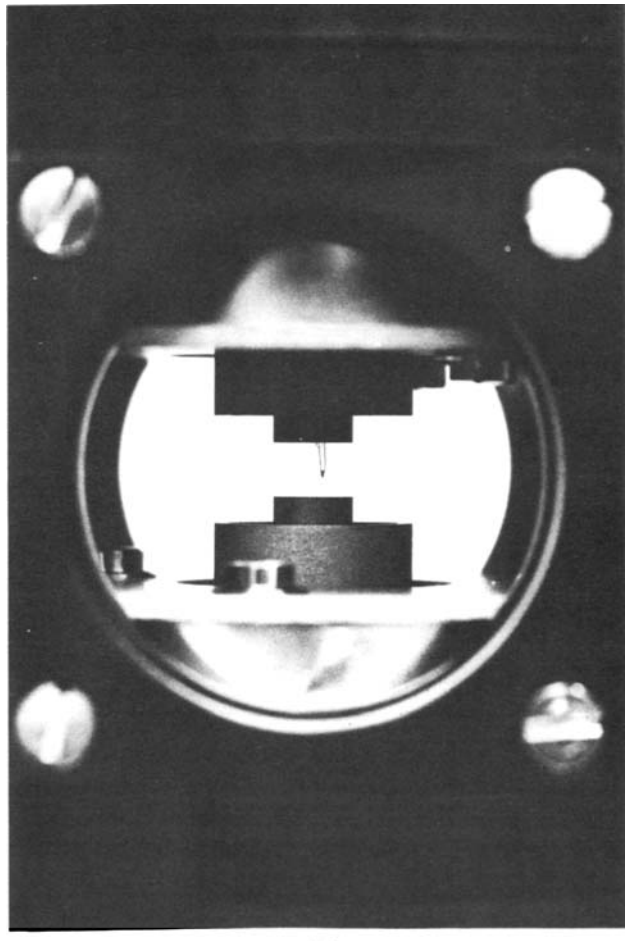

(b)

FIGURE 1. (a) Sectional drawing of the experimental chamber, 210 mm total length, 80 mm diameter in the middle region. (b) View through a chamber window of the 6 mm diameter graphite rods (without liquid zone); thermocouple inserted through the upper rod.

$l^2\chi \approx 100$ s of a fluid zone with a typical length of 4 mm. In quasistatic experiments the temperature difference was increased linearly in time at a rate of 0·1 K min^{-1} or less.

An important problem is the production of defined temperature boundary conditions in the free surface. The existence of the applied vertical temperature gradient is ensured by the great difference in the thermal conductivities of graphite and sodium nitrate. However, the radial heat flux out of the zone surface into the ambient gas is not negligible, since the thermal conductivity of air is significant ($\lambda(\text{air}) \approx \frac{1}{10}\lambda(NaNO_3)$) and heat radiation also contributes. In special experimental runs these radial temperature gradients have been minimized with a coaxial quartz tube with an inner diameter 4 mm larger than the zone diameter. The quartz tube was placed between the two graphite elements. As quartz and liquid $NaNO_3$ have similar thermal conductivities, the tube imposes the applied vertical temperature gradient on the zone surface.

In the zone, laminar flows are axially symmetric. This three-dimensional flow pattern is optically reduced to a two-dimensional one by a light-cut technique: a light band produced from a 5 mW He–Ne laser and some optics illuminates the zone in a vertical central section of 0·5 mm width only, and observations are made normal to it. The streamlines are indicated by trajectories of suspended particles (hollow quartz spheres, Eccospheres) with 0·01 mm average diameter. The streak lengths of the tracers and their motions have been used for streamline photographs and for most stream-velocity measurements. The observation of fluid motion in the zone interior is complicated because the zone liquid (refractive index $n(NaNO_3) = 1{\cdot}46$) acts as a cylinder lens itself and distorts the zone coordinates non-linearly. This was taken into account and corrected for all locations in the velocity and temperature measurements.

The temperature distributions and temperature oscillations have been determined with thermocouples of a platinum–noble-metal alloy with 0·05 mm wire diameter and approximately spherical thermojunctions of 0·15 mm diameter. The thermocouples are inserted either through the zone surface or, for the sake of an undisturbed free surface shape and surface-tension gradient, through a small bore in the upper graphite rod. The time constant of these thermocouples can be estimated to be 0·02 s. Confirmation of the thermocouple measurements of the surface temperature has been obtained with a non-contacting method using a highly focused high-speed bolometer (spatial resolution 1·0 mm) from Heimann.

3. The stationary flow pattern, temperature distribution, and stream velocities

In this section, typical features of time-independent TC and natural convection will be reported for zones with radius $a = 3{\cdot}0$ mm and A close to unity. The zones are heated from above to exclude buoyant convection in a vertical, unstable temperature gradient. Figure 2(*a*) shows the axially symmetric flow pattern of TC. The vertical surface-tension gradient drives a rapid surface flow ($v_z \approx 12$ mm s^{-1}) from the upper to the lower graphite rod in a surface layer with thickness $\delta \approx 0{\cdot}6$ mm. The typically sickle-shaped backflow from the lower to the upper rod in the bulk is recorded better, because the lens effect of the zone optically contracts peripheral regions. The maximum value of the surface velocity can be estimated to be four times that of the backflow speed. The corrected radial position of the roll axis is $R = 0{\cdot}85$, indicating the driving force to be located in the free surface.

Keeping the zone dimensions constant, the flow pattern of TC depends slightly on

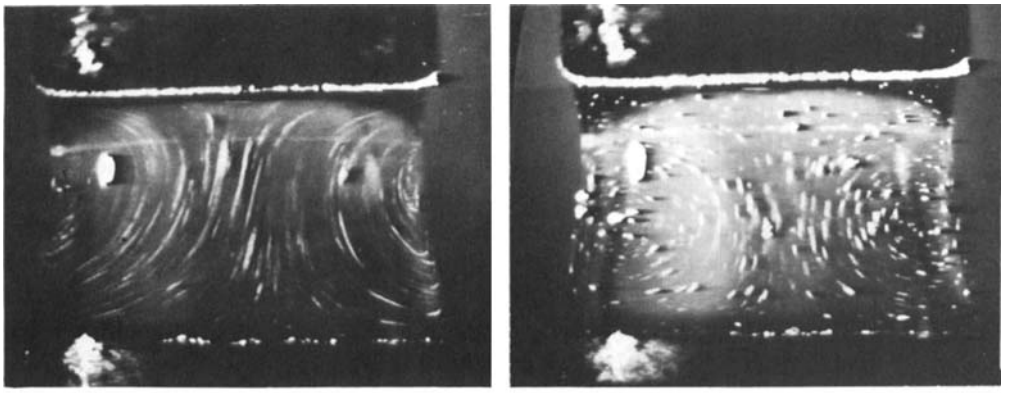

(a) (b)

FIGURE 2. (*a*) Dominating TC in a zone with clean and free surface; heated from above ($l = 4{\cdot}1$ mm, $a = 3{\cdot}0$ mm, $\Delta T = 10$ K, $Ma = 4{\cdot}8 \times 10^3$, exposure time $\frac{1}{8}$ s). (*b*) Same thermal conditions and exposure time as in (*a*), but TC is suppressed by a viscous surface film.

the Marangoni number. With increasing Ma the distance between vortex centre and surface decreases in accordance with the flow boundary-layer theory. The Prandtl relation has been confirmed quantitatively for TC by Schwabe (1981*b*). Above a Marangoni number of the order of 10^4, TC becomes oscillatory in space and in time; this will be discussed later.

As the average temperature of the melt is 355 °C, the periphery of the zone is cooled, thus producing a temperature gradient between zone surface and zone axis. By eliminating the thermocapillary forces with a surface contamination, it has been confirmed that the contribution of buoyant forces to the observed flow is small (Schwabe, Scharmann & Preisser 1980, 1982). In a further experiment the cooling conditions have been changed with a quartz cylinder placed between the heating rods and surrounding the zone. With free and clean surface, the flow speed of TC in the free surface remained ≈ 12 mm s^{-1}; with a contaminated surface, the flow speed of basic flow (BF) was $v_{\max} \approx 0{\cdot}1$ mm s^{-1}, indicating that radial temperature gradients have become small. These experiments show that two driving mechanisms are simultaneously present in the zone. However, TC dominates the buoyant convection in the case of a free and uncontaminated surface.

Measurements of the temperature distributions for dominating TC and for BF confirm the results gained from the flow pattern (figures 3 and 4). The isotherms have been drawn according to a grid of 12×12 temperature measurements in a vertical half-section of the zone. The temperature boundary layers near the graphite rods have been measured in special experimental runs and are taken into consideration in a first approximation.

A strong contribution of TC to heat transport can be seen in figure 3. The fast surface flow starting from the rim of the upper rod draws off the thermal boundary layer and bends the isotherms downwards, so that the surface is hotter than the interior. Near the middle of the zone the surface flow widens and penetrates into the bulk, thus bulging the isotherms.

The isotherm pattern produced by overwhelming TC is in good qualitative agreement with calculations for TC in a horizontal container with similar aspect ratio (Babskiy, Sklovskaya & Sklovskiy 1975). TC typically bends the isotherms near the free surface, whereas the backflow does not affect the isotherms up to considerable Marangoni numbers. This asymmetry is a feature of the surface character of TC. The

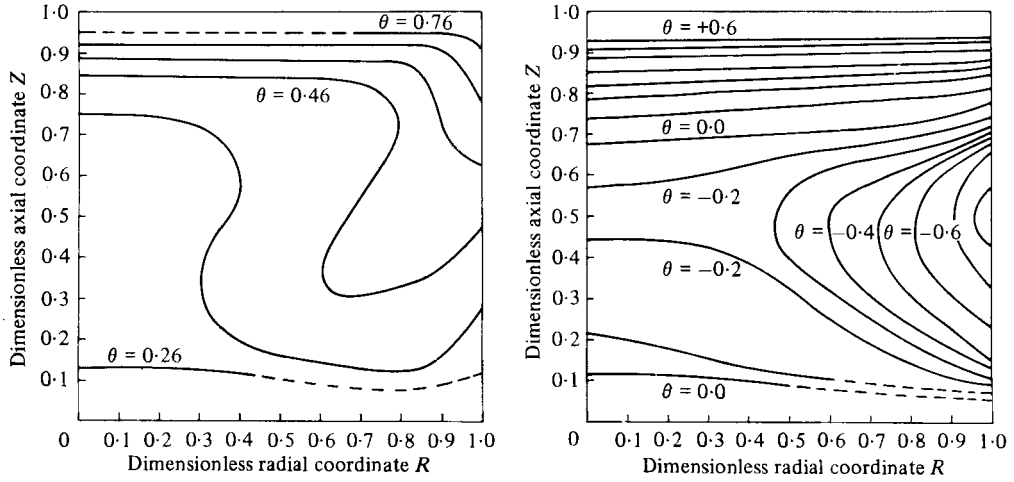

FIGURE 3. Isotherms in the vertical half of the zone shown in figure 2 (conditions as in figure 2).

influence of radiative cooling on TC has been taken into account theoretically in calculations by Chang, Wilcox & Lefever (1979) for the floating-zone crystal-growth technique of a high-melting-point material. They find similar behaviour of the radial temperature curves, and, in addition, the surface flow is directed slightly radially inwards. The temperature distribution has also been determined for higher Marangoni numbers (figure 4). When TC is oscillatory the time-averaged temperature has been taken at each measuring point. At $Ma = 2 \times 10^4$ the vigorous TC determines the temperature field completely. As is to be expected, the thermal boundary-layer gradients become steeper at the cold end and the surface isotherms are bent markedly downwards.

One of the conclusions to be drawn from the temperature measurements is the fact that buoyant forces are always significant compared with thermocapillary forces in a zone of this size. The stabilizing forces in heating from above (or destabilizing under heating from below and due to horizontal temperature gradients) are always present. They become small compared with thermocapillary forces for zone length $l \leqslant 4$ mm.

In figure 5 the radial velocity distribution of laminar TC is given at axial position $Z = 0{\cdot}68$. The geometrical conditions and the Marangoni number allow correspondence with the previous figures. It is shown that the downward surface stream is restricted to a narrow boundary layer with a maximum flow speed of 12 mm s^{-1}. Because of the optical distortion, measurements are difficult in the periphery of the zone, and the local resolution is limited there.

The existence of a radial maximum of the speed of the backflow at $R \approx 0{\cdot}4$ indicates that TC is limited to a region near the free surface. The radial dimension of this region (called the penetration depth of TC) scales as the length of the zone. With increasing *Ma* the position of the backflow-speed maximum penetrates deeper into the interior. The smooth decrease towards the zone axis is due to the combination of BF and TC that will be pointed out clearly in the discussion of figure 7. This velocity-distribution measurement is in agreement with data from a horizontal boat (Schwabe & Scharmann 1981).

To study the kinematical behaviour of TC, its stream velocity was measured as a function of the applied temperature gradient along the surface and the Marangoni number. The axial stream velocity of TC is given in figure 6 for two different zone

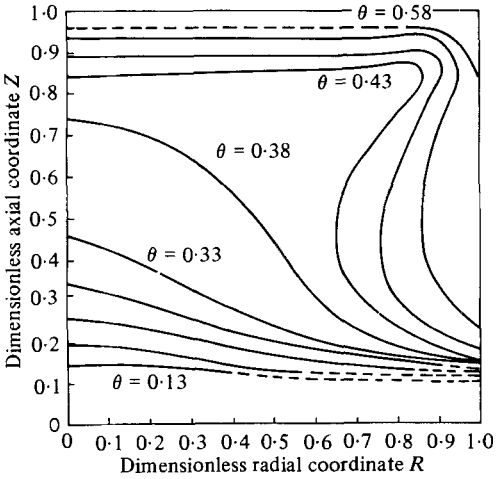

FIGURE 4. Isotherms in a vertical half of the zone at higher Marangoni number; $l = 4{\cdot}1$ mm, $a = 3{\cdot}0$ mm, $T_{\text{upper}} - T_{\text{lower}} = 40$ K, $Ma = 1{\cdot}9 \times 10^4$.

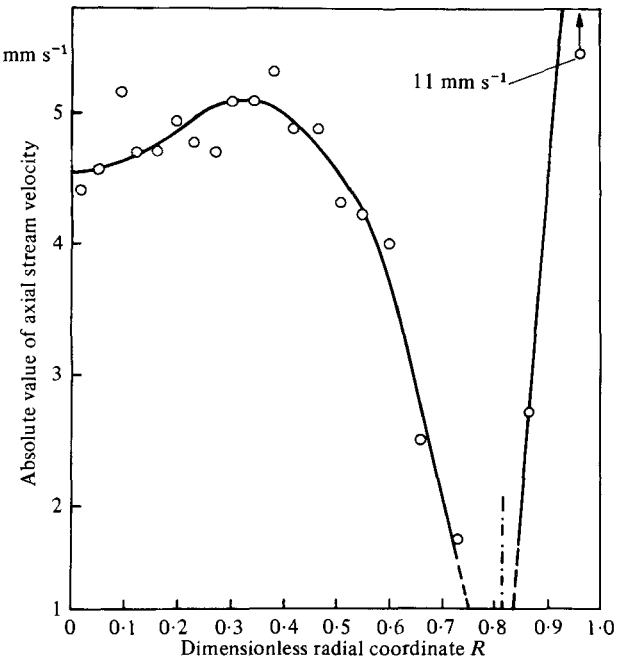

FIGURE 5. Radial velocity distribution of TC at zone height $z = 0{\cdot}68$; $l = 4{\cdot}1$ mm, $a = 3{\cdot}0$ mm, $\Delta T = 10$ K, $Ma = 4{\cdot}8 \times 10^3$; dashed line indicates radial position of roll axis (point of zero velocity).

lengths. If the stream velocity is plotted versus the vertical temperature difference ΔT, the curves for both zone lengths coincide within the limits of error. The flow speed of TC in the experiments under consideration is proportional only to the temperature difference parallel to the free surface. If the zone length is constant, the measured stream velocity depends linearly on the Marangoni number, as can be seen in figure 6(*b*). The linear dependence on *Ma* seems to be a significant difference from buoyant convection, where the flow speed is related to the square root of the Rayleigh number. This proportionality over the one order of magnitude shows that the Marangoni

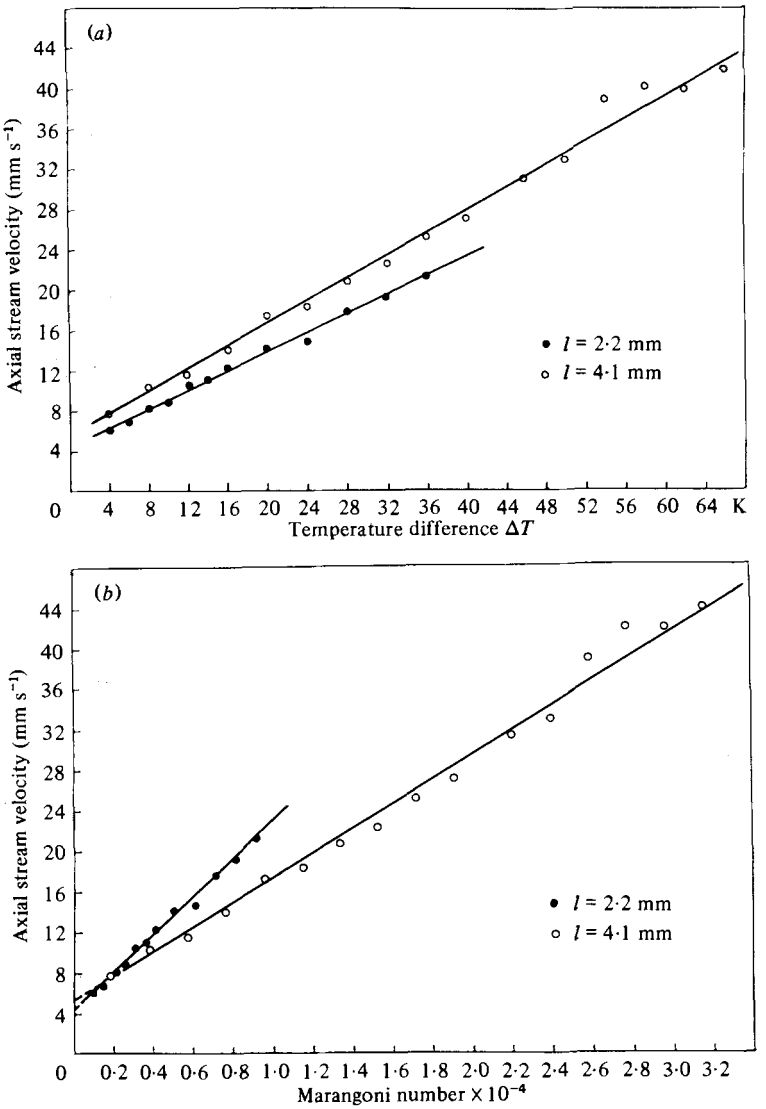

FIGURE 6. Stream velocity of TC in the free surface ($R = 1$); measurements performed between $Z = 0{\cdot}9$ and $Z = 0{\cdot}6$ in zones with $a = 3{\cdot}0$ mm.

number, as defined by (1), is the appropriate non-dimensional quantity to describe TC in the present experiment, and that the influence of buoyant forces can be neglected in the surface flow when $Ma \gg 0$.

As can be seen in figure 6 by extrapolation of $Ma \to 0$, the stream velocity does not vanish, as it should for $\Delta T \to 0$ if thermocapillary forces were acting alone. This is due to the heating conditions in this experiment: although ΔT between the graphite rods is adjusted to zero, temperature gradients along and normal to the surface are caused by radial cooling, thus driving combined TC and buoyant convection.

Figure 7 shows the stream velocity of the upward backflow on the zone axis as a function of Marangoni number. In the case of unaffected TC, its backflow speed is expected to be proportional also to ΔT, because of continuity requirements. This is verified for large Ma, but for small Ma surprisingly the velocity is constant. The

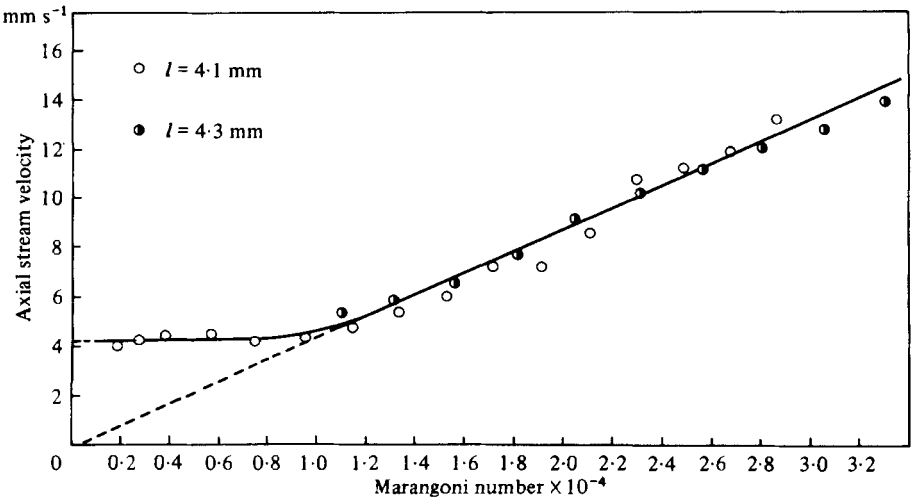

FIGURE 7. Stream velocity at the axis ($R = 0$) of zones with $a = 3{\cdot}0$ mm; measurements taken between $Z = 0{\cdot}35$ and $Z = 0{\cdot}65$. (Data for $l = 4{\cdot}3$ m have been obtained with a laser-Doppler anemometer.)

latter feature is caused by the radial cooling of the zone, because at small Ma the downward surface stream is not strong enough to compensate for the radial heat flux. In a first approximation the resultant BF velocity is independent of the applied vertical temperature difference and dependent on the approximately constant lateral cooling conditions only. As indicated by the dashed line, the extrapolation of the stream velocity from higher Ma to $Ma = 0$ does give a zero value. This demonstrates that TC also dominates in the interior of zones with 6 mm diameter if $Ma > 10^4$.

4. The flow pattern in zones with aspect ratio < 1

If the aspect ratio is reduced to values of the order of 0·1, the flow pattern changes drastically. As is demonstrated in figure 8 for a zone with $A = 0{\cdot}47$, the TC roll (downward and upward flow) is confined to the zone periphery and in the interior an axially symmetric roll of BF merges with the TC-vortex. In figure 8(a) the exposure time was 4 s in order to show the motion of the inner BF-roll, whose velocity ($v_{max} \approx 0{\cdot}2$ mm s^{-1}) is one order of magnitude lower than the TC backflow speed. Therefore the TC stream pattern cannot be resolved spatially in the photograph and the vortex appears as a semicircular disk. Although the zone is heated from above, radial temperature gradients cannot be excluded in the bulk: at the axis the axial temperature profile is governed by conduction, whereas in the periphery the TC produces thermal boundary layers, as can be seen in figures 3 and 4. This resultant radial temperature gradient drives BF. It must be emphasized that the radial cooling of the zone surface, which gives rise to a contributory buoyant force (BF), as discussed above is almost eliminated by the TC flow in this experiment. The convective heat transport by TC itself maintains buoyant convection in the bulk, because it determines the thermal boundary conditions of the zone interior.

Observations have shown that the overall flow pattern or the ratio of volumes occupied by TC and BF, respectively, depend on the aspect ratio. If A is decreased to smaller values in comparison with figure 8(a) surface flow and backflow of TC are increasingly confined to a thin layer near the free surface. It has been found for $l \leqq a$ that the radial penetration depth of TC is of the order of the length of the zone.

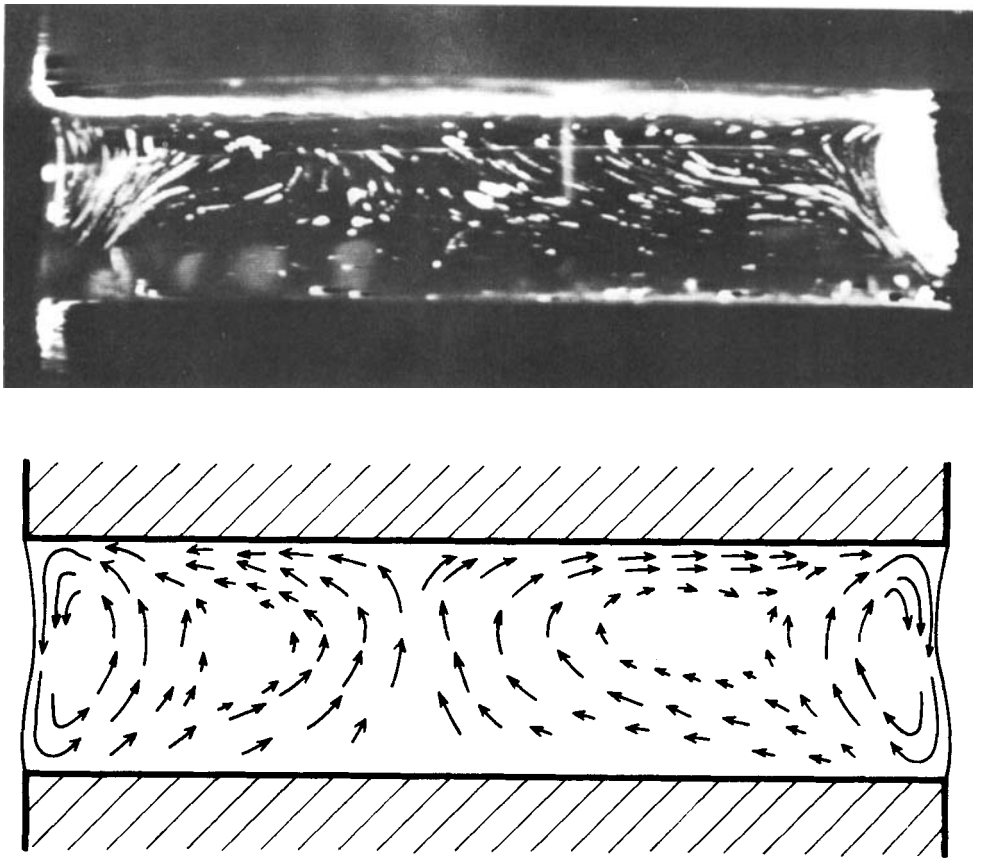

FIGURE 8. TC in the periphery and BF in the interior of a zone heated from above with $A = 0{\cdot}47$, $a = 10{\cdot}0$ mm, $\Delta T = 11$ K, exposure time 4 s. (*a*) Photograph, (*b*) sketch of the flow pattern.

5. The oscillatory instability of TC

5.1. *Description of the flow pattern*

When a certain Marangoni number (critical Marangoni number Ma_c) is exceeded, TC shows a transition to three-dimensional motion. The flow pattern becomes periodic in space and in time, so that this state has been named the oscillatory TC (Schwabe *et al.* 1978; Schwabe & Scharmann 1979; Chun & Wuest 1979). In figure 9 the streamlines of oscillatory TC on the zone surface and in a vertical section are sketched for a fixed time. The moment is depicted when the vortices (rolls) in the light cut have extreme positions (figure 9*b*). The vortex in one half of the zone section appears smaller than the opposite vortex, and the centre of the smaller vortex is located nearer to the lower solid boundary. The larger vortex is characterized by a centre closer to the upper graphite rod. In the light cut the time dependence is observed as periodical interchange of the shape of the vortices in the left and right parts of the zone. After one half of the oscillation period the left vortex (small) and the right vortex (large) have changed positions. In the total view in figure 9(*a*) the time dependence is described with the movement of the branching streamline of opposite vortices. The branching streamline rotates with the oscillation frequency around the zone axis in the surface of a cone. While the features of the laminar TC roll are independent of the azimuthal angle, the oscillatory state at a fixed time is characterized by a

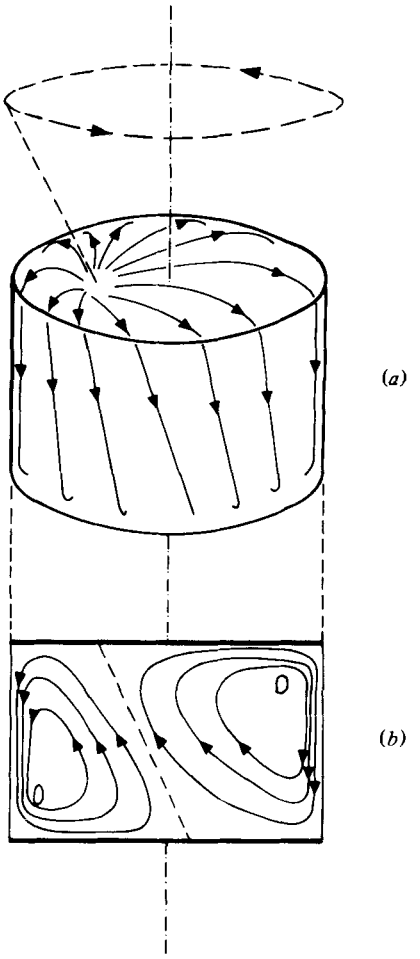

FIGURE 9. Qualitative picture (at fixed time) of the oscillatory TC with mode number $n = 1$ (as in a zone with $l \approx 5{\cdot}0$ mm, $a = 3$ mm). The distortion of the TC roll travels around the zone axis (direction of propagation arbitrary). (*a*) Streamlines in the surface (upper and lower graphite rod removed, branching streamline as broken line). (*b*) Flow pattern in the vertical light cut.

sinusoidal distortion of the roll cross-section and the roll axis in azimuthal direction. The time dependence is caused by the propagation of this distortion around the zone axis. Therefore the instability is recorded as a flow oscillation in the fixed light cut or as a temperature oscillation with a stationary themocouple. This appearance of instable TC has also been observed in liquid zones with $Pr = 0{\cdot}27$ (Schwabe *et al.* (1979) and $Pr = 7{\cdot}1$ (Chun & Wuest 1979).

The symmetry of the zone makes the assumption plausible that only an integer number n of periodical roll distortions can develop on the circumference of the zone:

$$n\lambda = 2\pi a, \tag{2}$$

when λ is the real wavelength of the instability in the azimuthal direction. The integer n is called the mode number. In our experiments it has been found that mode number and wavelength are a function of the aspect ratio. In figure 9 the flow pattern for the lowest mode $n = 1$ has been described, and it is demonstrated in a photograph of a vertical light cut in figure 10. If the aspect ratio is decreased by reduction of the

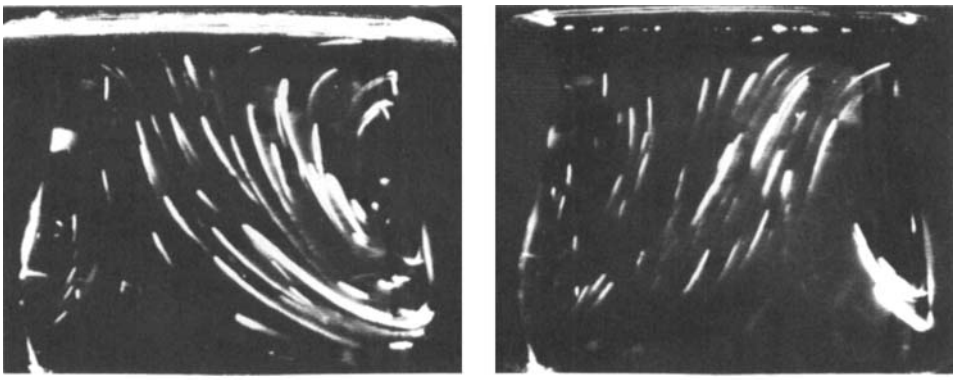

(*a*) (*b*)

FIGURE 10. Oscillatory TC with $n = 1$, recorded by the tracks of illuminated suspended particles in a zone with $l = 5{\cdot}4$ mm, $a = 3{\cdot}0$ mm (zone dimensions and mode correspond to figure 9). Time difference between (*a*) and (*b*) ≈ 1 s (oscillation period $\tau = 2{\cdot}0$ s): the left and right vortex interchange their positions after one half of the period.

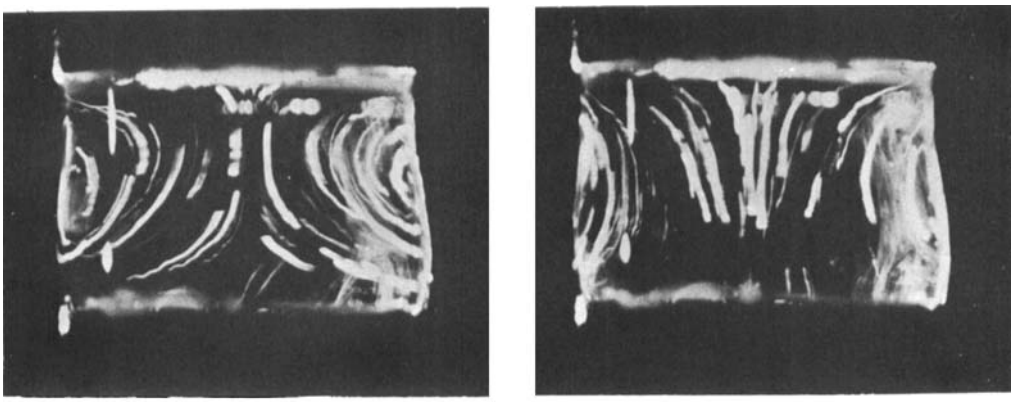

(*a*) (*b*)

FIGURE 11. Oscillatory TC with $n = 2$ in a zone with $l = 3{\cdot}5$ mm, $a = 3{\cdot}0$ mm. (*a*) and (*b*) have been taken at a time interval of half of the oscillation period, showing the two extreme distortions of the TC roll ($\tau = 1{\cdot}6$ s).

zone length, the mode $n = 2$ is observed for $0{\cdot}8 \leqq A \leqq 1{\cdot}3$. The mode $n = 2$ is characterized by a synchronous pulsation of the roll cross-section in the light cut, as can be seen in the photographs in figure 11. Higher modes were identified at corresponding lower values of A with the aid of a stereo microscope: a fraction of the suspended particles is always trapped in the wavy axis of the instationary TC roll, so that the wavelength of the oscillation can be measured roughly when the zone surface is observed. In the lower part of figure 12, mode numbers for the fully developed instability at $Ma = 1{\cdot}1Ma_c$ are given. A certain mode exists in a certain range of A, but for higher modes identification is difficult and sudden transitions to neighbouring modes can occur, which is indicated by the error bars. It is found that at constant zone radius the mode number increases with decreasing zone length. For zones of various diameters the modes depend on the aspect ratio in a unique way. In the upper part of figure 12 the product nA has been plotted. It gives the important experimental result that

$$nA \approx \text{const} \approx 2{\cdot}2 \quad (A \leqslant 1) \tag{3}$$

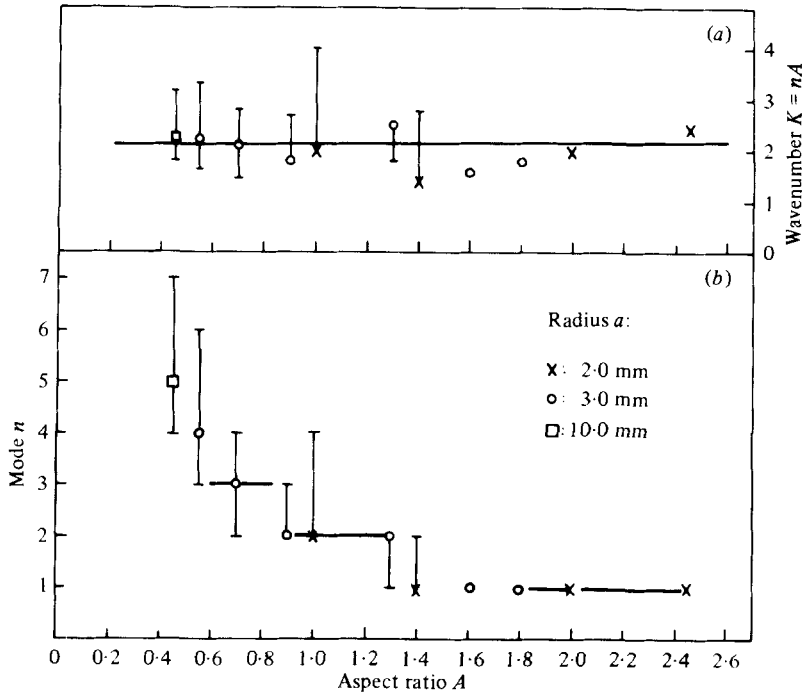

FIGURE 12. (*a*) The product nA is a characteristic constant of the oscillatory TC which is independent of zone aspect ratio. nA is the dimensionless wavenumber K of the instability. (*b*) Observed mode numbers of the developed instability at $Ma = 1{\cdot}1\,Ma_c$ in zones with different geometries.

for all zones. Combination of (2) and (3) gives the result that the wavelength λ of the oscillation is proportional to l and independent of a. The zone length l seems to be the only proper characteristic length in the description of oscillatory TC in zones with $l \leqq a$: It is convenient therefore to use a Marangoni number $Ma \sim l$ for the description of oscillatory TC, as defined before.

With the produce nA, a constant dimensionless entity for oscillatory TC has been found that provides a possibility of calculating mode numbers when A is given. The meaning of this constant can easily be understood, if one takes into account that the wavelength λ of the oscillation scales with the length of the zone, so that the non-dimensional wavelength Λ is written

$$\Lambda = \lambda l^{-1}. \tag{4}$$

Combining (2) and (4), the non-dimensional wavenumber K of the oscillatory TC at $Ma = 1{\cdot}1Ma_c$ is determined to be

$$K = 2\pi\Lambda^{-1} = nla^{-1} = nA \approx 2{\cdot}2. \tag{5}$$

In all zones the unstable TC developed a wavy structure with this wavenumber.

A peculiar problem concerns the mode transitions when the aspect ratio is changed, because there are intermediate ranges in A (continuous parameter) where either one mode (discrete parameter) or the other can exist. The oscillatory system seems to possess various degrees of freedom (penetration depth, azimuthal component of stream velocity) to lock into a main mode. The basic flow has also been recognized to be an important criterion for mode selection: a strong basic flow stabilizes the mode $n = 1$ down to smaller A, compared with the case of good radial thermal insulation.

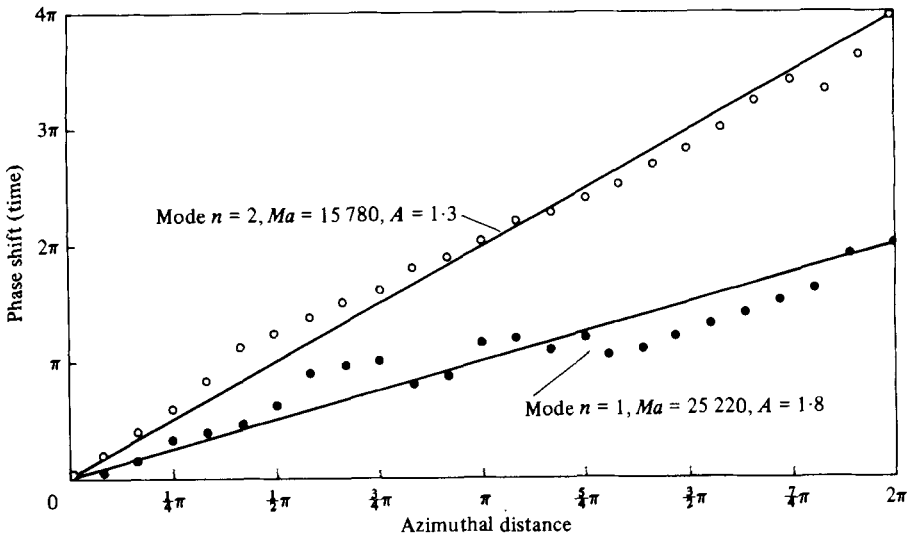

FIGURE 13. Phase shift (in time) of the temperature oscillations in a zone with $a = 3{\cdot}0$ mm, measured with two thermocouples.

A dependence of K on the Marangoni number in a zone with constant A could not be detected within the experimental conditions. After a certain mode had established at Ma_c, no mode transition was observed up to $5Ma_c$, although indications of frequency jumps and broadening of the spectrum occurred in the oscillation signal. The temperature oscillations coupled with the instability of the flow field are almost sinusoidal, which was indicated by the Fourier analysis showing a sharp main frequency with an amplitude orders of magnitude higher than its higher harmonics and the amplitude of noise (Preisser 1981; Schwabe, Preisser & Scharmann 1982; Schwabe, Scharmann & Preisser 1980, 1982).

From the azimuthal phase difference of the temperature oscillations, the existence of the modes $n = 1$ and $n = 2$ and their characteristic property as running waves were verified. The phase shift was measured as a function of the azimuthal angle between the positions of one fixed and one azimuthally movable thermocouple, both positioned at the same radial and axial coordinates. As can be seen in figure 13, the phase difference increases linearly with the azimuthal angle, and equals 2π for the optically recognized mode $n = 1$, and 4π for $n = 2$. As the temperature oscillations are independent of the azimuth in their amplitude and their form of signal, a standing wave is excluded.

However, the amplitude $\frac{1}{2}S$ varies spatially in every vertical (r, z)-plane, as is shown in figure 14. The maximum amplitudes are detected in the backflow, and typically have peak-to-peak values of 10 % of the applied temperature difference. Surprisingly, the amplitudes are smaller in the surface flow, with a tendency to decrease towards the bottom boundary. This result makes it reasonable to assume that the oscillations have their origin mainly in the radial displacement of stream paths. The alternate motion of the back flow radially inwards and radially outwards produces the maximum temperature fluctuations, whereas the surface stream sticks to the zone surface. Measurements of the surface temperature with a non-contacting bolometer have shown temperature oscillations in the free surface with amplitudes of typically about 5 % of the applied ΔT.

A further possible interpretation of the temperature fluctuations is as circulating

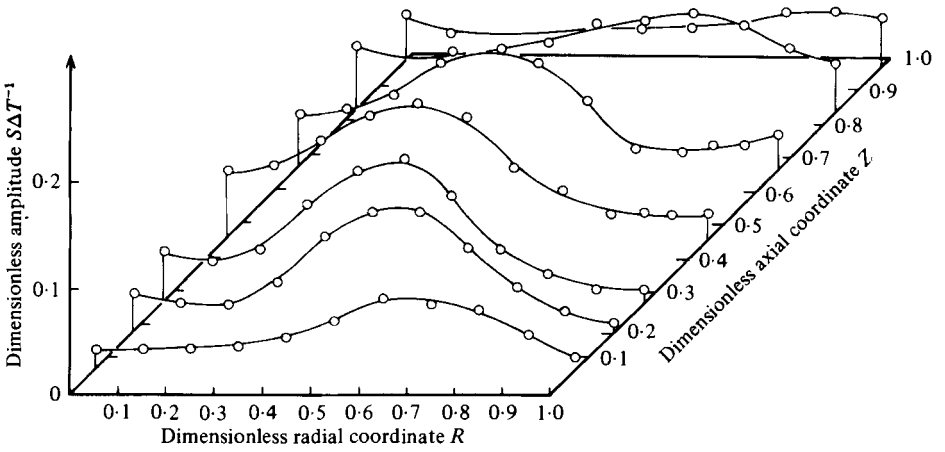

FIGURE 14. Spatial variation of the oscillation amplitude in a vertical cross section of the oscillatory TC roll; $l = 4{\cdot}1$ mm, $a = 3{\cdot}0$ mm, $\Delta T = 40$ K, $Ma = 1{\cdot}9 \times 10^4$; amplitude normalized with the vertical temperature difference ΔT.

hot or cold spots that are periodically released in boundary layers and are transferred by the convection roll, thus generating an oscillating temperature at a fixed point. According to this model the amplitude should be fairly constant in the downward or upward flow. However, figure 14 shows the maximal amplitude to be in the middle of the zone. Furthermore, a number of thorough measurements with two thermocouples at equal azimuthal angle have failed to show an axial phase shift of temperature oscillation either in the surface stream or in the backflow. However, it cannot be excluded that thermal spots exist with amplitudes below the detection limit. They could distort the surface-tension gradient and thus cause the pulsations of the convection roll. Thermal oscillations in the free surface exist in any case, as shown by the bolometer measurement. Surface oscillations with the frequency of oscillatory TC are clearly shown in the light reflected by the free surface.

Summarizing the observations and the previous measurements, the picture of the oscillatory TC is described as follows: the oscillation consists of a periodical radial and axial fluid motion throughout the length of the zone, suprimposed on the continuous convective motions, which lie approximately in vertical planes. Because of the surface boundary conditions only the radial displacement of the backflow in the bulk is clearly pronounced. In the backflow, oscillations are nearly in phase in every vertical section of the TC roll, and phase shifts occur in the azimuthal direction. The time dependence is caused by the propagation of the radial motion along the circumferential roll axis. In a more-detailed description of the oscillatory state some more experimental observations have to be included, e.g. that temperature oscillations show a phase jump of $\frac{1}{2}\pi$ between downward and upward flow in a vertical plane near the lower solid rod, and that oscillatory azimuthal velocity components clearly exist in the surface flow and in the backflow.

5.2. *The onset of the instability*

The critical value for the transition from laminar TC to the oscillatory state has been determined for different zone sizes by measuring the onset of thermal oscillations. The vertical temperature difference is slowly raised linearly in time under quasistatic thermal conditions, and the increase of the amplitude $\frac{1}{2}S$ is recorded. Figure 15 shows a typical result of an experimental run: below a certain Ma_c no oscillations occur,

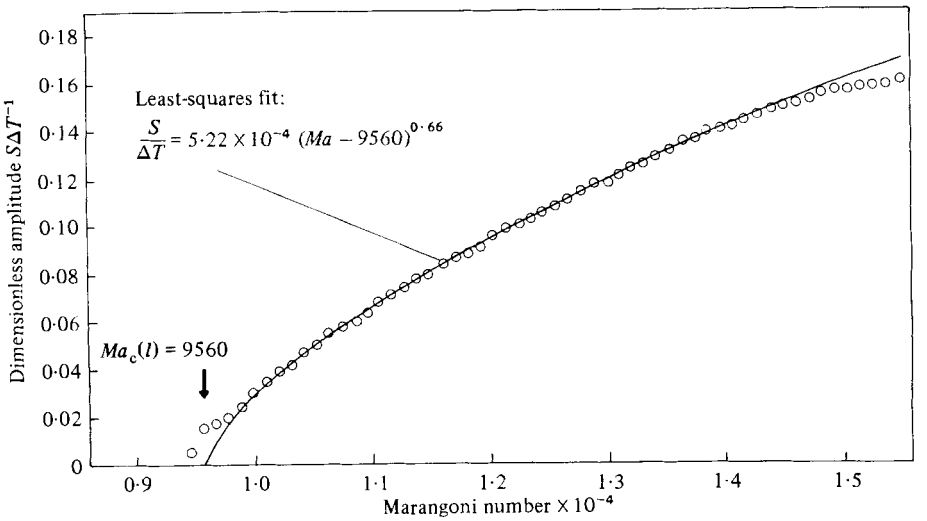

FIGURE 15. Increase of the normalized amplitude of temperature oscillations in a zone with $l = 4{\cdot}6$ mm and $a = 3{\cdot}0$ mm. The functional dependence $S\ \Delta T^{-1} = \text{const} \times (Ma - Ma_c)^x$ is fitted to experimental values. The critical Marangoni number is obtained from the extrapolation of this function.

at Ma_c oscillations begin, and from $1{\cdot}05Ma_c$ the normalized amplitude grows continuously. The functional dependence of the amplitude on the Marangoni number in the range $Ma < 1{\cdot}5Ma_c$ has been fitted with power functions of the form

$$S\Delta T^{-1} = \text{const} \times (Ma - y)^x. \tag{6}$$

In (6) the constant, $y \equiv Ma_c$ and x are determined by a least-squares fit. The averaged value of the growth exponent x from a series of experiments with different zone lengths was found to be $x \approx 0{\cdot}5$. Any explanation of the instability must take into consideration this growth exponent together with the linear dependence of the stream velocity on the Marangoni number.

With the aid of the growth exponent 0·5 the critical Marangoni number was obtained by linear extrapolation of the amplitude to zero when the amplitude was plotted versus the square root of the Marangoni number. The critical Marangoni number in zones of widely varying geometry is given in figure 16. For zones with $l \leqq 3{\cdot}5$ mm it is a constant, as it has been indicated in preliminary work (Schwabe & Scharmann 1979), and Ma_c turns out to be independent of the mode of the instability:

$$Ma_c = (7{\cdot}4 \pm 1{\cdot}4) \times 10^3.$$

Ma_c is also independent of radius.

The increase of Ma_c with l in the longer zones is interpreted as stabilization due to radial temperature gradients, because the lateral heat flux into the environment of the zone increases with the zone length. The stabilizing influence of radial temperature gradients could clearly be verified in successive experiments with either a water-cooled tube, or an insulating quartz cylinder, surrounding the zone. For the same zone length the critical Marangoni number increased by $\sim 10\%$ in the case of strong radial cooling and decreased by $\sim 10\%$ under radial thermal insulation, both values compared with the usual experimental conditions. The stabilizing tendency of BF is thought to be due to its influence on the vertical temperature gradient (decreasing it). Furthermore, BF reduces velocity gradients, because the body forces

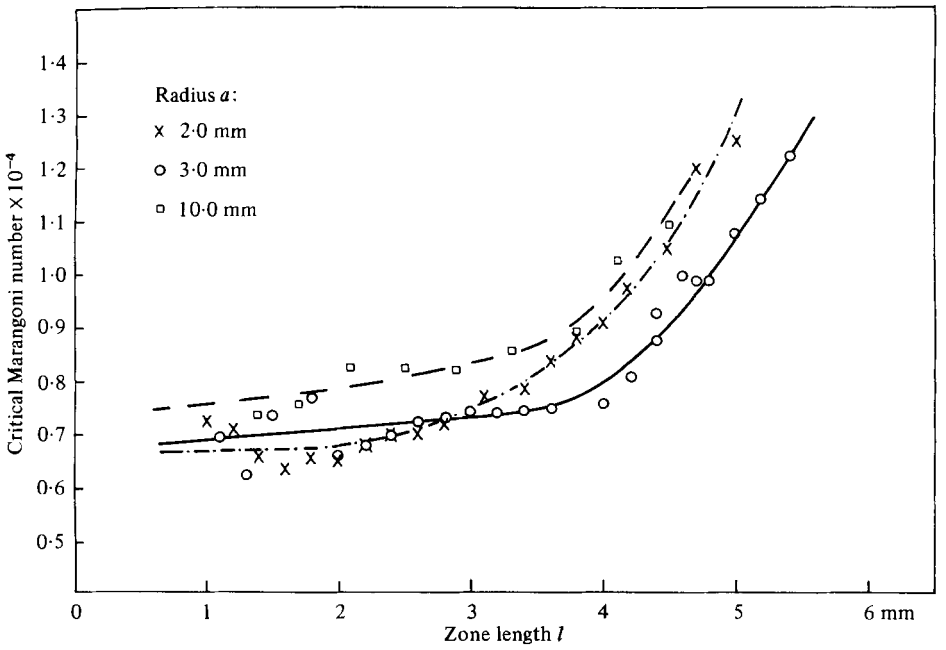

FIGURE 16. Critical Marangoni number for the transition to the oscillatory flow state of TC in zones of different size.

tend to widen the surface-flow layer and to enhance the radial penetration depth of the backflow.

5.3. *Analysis of the temperature oscillations*

To get further information on the oscillatory state, the frequencies of the temperature fluctuations were measured as a function of zone length, radius and over-temperature ΔT or Marangoni number. The zone length has the determining influence on the frequency. As shown in figure 17, the frequencies increase strongly with decreasing zone length in a similar way for all radii, and the same tendency exists for constant length and decreasing radius. Previous rough determinations of the frequency dependence by Schwabe *et al.* (1978) are confirmed here. In addition the curves have been fitted with power relations $f = \text{const} \times l^z$, and the fit for zones with $a = 3{\cdot}0$ mm is shown in figure 17. It was found that $z \approx -1{\cdot}5$, if the frequencies for $l > 3{\cdot}5$ mm are considered with a weighting factor smaller than 1, because in long zones BF influences both Ma_c and f.

The non-dimensional frequency

$$F = f\chi l^{-2} Ma^{-\frac{1}{2}} \tag{7}$$

has been found to be the most suitable to represent the experimental results for zones of different size (figure 18). The thermal diffusion times enters the expression for F because thermal effects should not be excluded at $Pr = 8{\cdot}9$. $Ma^{-\frac{1}{2}}$ is chosen as a factor because for constant zone dimension the frequency f increases with Ma raised to a power between 0·5 and 1, as mentioned below. The defined F is independent of the zone size, if the aspect ratio is constant (figure 18). The representation is valuable, because geometric parameters drop out completely for constant A (e.g. see $A \approx 0{\cdot}45$ in figure 18). However, the dimensionless frequency F still depends linearly on the aspect ratio. Since the wavenumber K has been found to be approximately constant,

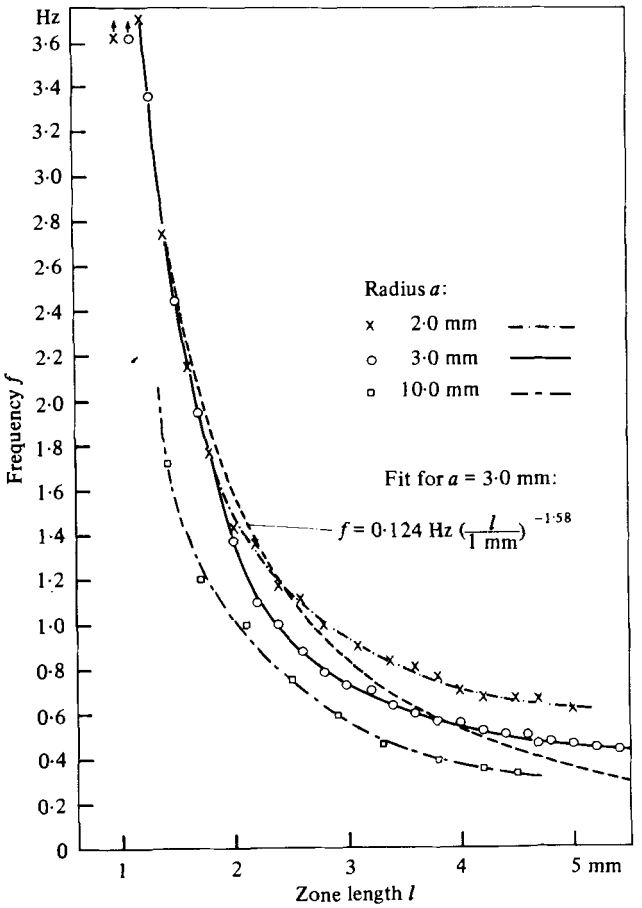

FIGURE 17. Frequencies of temperature oscillations measured at $Ma = 1{\cdot}1\,Ma_c$ in zones of different size.

this means that the dimensionless phase velocity $V_p = 2\pi FK^{-1}$ for the travelling wave increases with A. Since $A = Kn^{-1}$, it follows that disturbances with higher mode numbers propagate slower than those with smaller n, even in the case of equal zone length. The decrease of the frequency and the phase velocity with A is thought to be due to variations of the averaged flow speed in the bulk because of two reasons:

(i) with decreasing A, the ratio between the free surface and the horizontal boundaries also decreases, so that damping shear stress exerted by the rigid boundaries becomes more important;

(ii) in zones with $A > 1$, the backflow is bounded by itself at the zone axis so that the axial back flow speed is enhanced. Thus a damping of the averaged fluid motion is expected for small A, which is recorded as a lower propagation speed.

The dependence of the frequency on the Marangoni number under constant zone dimensions could not be obtained very accurately. The frequency increases with the Marangoni number raised to a power between 0·5 and 1 (Schwabe 1981*b*).

6. Concluding remarks

The previous experiments have shown that TC can be a strong convection phenomenon which dominates buoyancy-driven convection in volumes up to

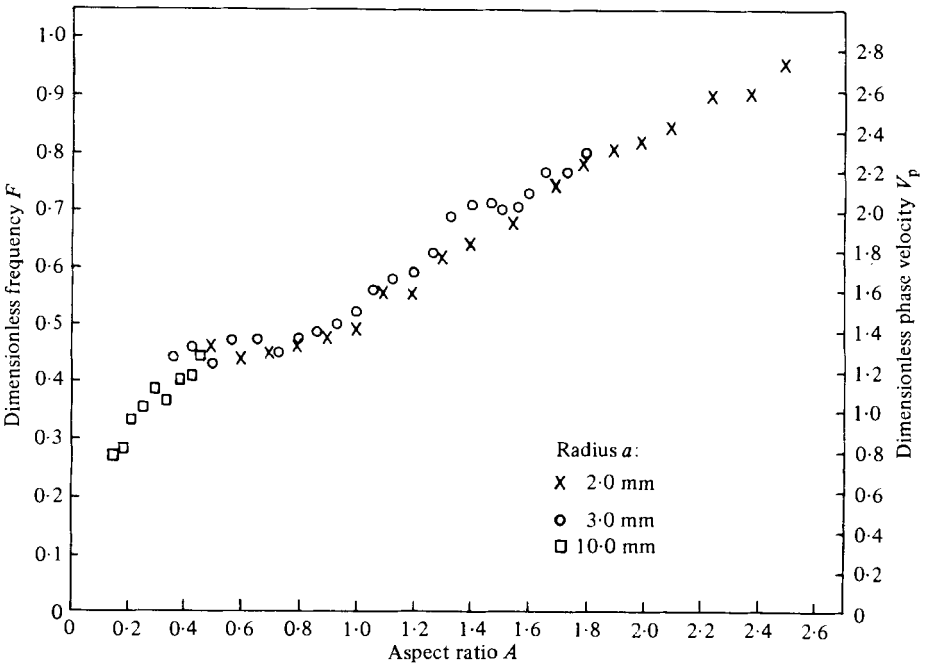

FIGURE 18. Dimensionless frequencies $F = fl^2\chi^{-1}\, Ma^{-\frac{1}{2}}$ at $Ma = 1{\cdot}1\, Ma_c$. Right ordinate gives the propagation speed of the instability obtained by $V_p = 2\pi FK^{-1}$, thus showing the existence of a dispersion relation in A.

approximately 1 cm^3. The flow pattern in zones with $A \approx 0{\cdot}1$ exhibits an important property of TC and indicates the limits of TC for bigger volumes: as TC is a surface phenomenon, it will be confined to a region near the surface, whereas body forces determine fluid motion in bulk.

Besides the magnitude of TC the existence of an oscillatory instability triggers the particular interest in TC. The toroidal roll cell undergoes defined and pronounced deformations, which are rather insensitive to preheating conditions and thermal disturbances in the ambient air and in the liquid itself (thermocouples). It seems that discrete wavenumbers of disturbances are selected out of the full spectrum of disturbances, because the convection roll is closed in the special zone geometry. Non-fitting disturbances are eliminated by destructive interference. The selection rule is given by the constraint that the wavelength must be an aliquot of the zone circumference. However, the physical mechanism that amplifies and feeds the flow disturbance is still uncertain. Chun & Wuest (1979) claim the oscillations to be due to an overstable interaction between flow and temperature field in the surface of the zone.

There are two different existing theoretical models that can possibly be adopted for the qualitative description of oscillatory TC and can perhaps contribute to the understanding of its origin. On the one hand there is the theory for the oscillatory instability of convection rolls of Busse (1972) and Clever & Busse (1974), and on the other hand the instability of two-dimensional thermocapillary shear flow by Smith & Davis (1981).

Since Busse's model should be valid for any field of two-dimensional vortices, attempts to draw analogies should be successful despite the great differences in the boundary conditions and despite some particularities due to the action of surface-tension gradients. Following Busse, the oscillation of the TC roll can be interpreted

in a first approximation as a propagating periodical lateral shift of the axis of the undisturbed roll. As the roll sticks to the zone surface, only the motion radially inwards is clearly observed as pulsations of the roll cross-section. The picture could explain why the maximum amplitude of temperature oscillations was found at medium zone heights and why our attempts to identify vertically circulating thermals were fruitless, much in the same way as was found for oscillatory Rayleigh–Bénard convection by Willis & Deardorff (1970). With the aid of the frequency dependence (Busse 1972) the measured frequencies of oscillatory TC are reproduced when $(Ra - Ra_c)/Ra_c$ in the expression for F is replaced by the Marangoni number Ma (as the Marangoni number for the onset of TC is zero, this simple substitution seems to be obvious). This gives (7). The linear dependence of the non-dimensional frequency on the aspect ratio, however, resembles a pecularity of TC in the zone: as the roll is closed, the instability is additionally coupled in the azimuthal direction by periodical distortion of the surface-tension gradient. If the TC roll is linear, e.g. in a zone with $a = \infty$, this coupling condition can be dropped and the frequency must become independent of A and depend on l as the sole geometrical parameter. Indeed, the extrapolation of the curve in figure 18 for $A \to 0$ gives a constant non-dimensional frequency, which means that the zone length is the sole dimension determining the frequency in this limit. Discussing oscillatory TC within the framework of Busse's analysis, it cannot be excluded that the finer details of oscillatory TC are due to azimuthal surface-tension gradients. The build up of oscillatory azimuthal temperature gradients (and surface-tension gradients) is a direct consequence of the running wavy disturbance in the axial and radial velocity component.

Very recently Smith & Davis (1981) have shown that thermocapillary convection in a trough becomes unstable to waves in the surface flow. Although there is some correspondence between the calculated critical Marangoni numbers and wavenumbers with the experimental findings in this work, it is not easy to reconstruct the oscillatory flow pattern in the zone with this two-dimensional model. TC exhibits the wavy structure mainly in the azimuthal direction of the zone, which is topologically related to the direction not considered in this two-dimensional model. The possibility of a wave normal to the surface flow, propagating by oscillations of the surface flow itself, as observed in our experiment, should be investigated in this model.

With an experiment in the German sounding rocket project TEXUS the authors of the present paper have proved that the oscillatory state of TC is a gravity-independent instability (Schwabe, Preisser & Scharmann 1982; Schwabe, Scharmann & Preisser 1980, 1982). Two transcritical Marangoni numbers ($Ma = 1{\cdot}6 \times 10^4$ and $3{\cdot}6 \times 10^4$) were applied to a zone during the microgravity phase ($10^{-4}g$) and the temperature oscillations due to oscillatory TC were recorded. The Fourier analysis showed that the same main frequency with the same higher harmonics and with the same amplitude ratios occurred as in the laboratory reference experiment. Overstable interactions of TC with buoyant convection or gravitational instationary boundary layers are excluded as the origin of oscillatory TC.

This work represents part of the thesis of F. Preisser at Giessen (1981, D26), and is dedicated to Professor Dr D. Hahn, PTB Braunschweig, on the occasion of his 60th birthday.

The authors gratefully acknowledge support by the Federal Ministry for Research and Technology of the FRG under contract no. 01 QV 148-ZA-SN-SLN-7786-3-7, and supply with graphite of highest quality by Schunk & Ebe GmbH, Giessen.

REFERENCES

BABSKIY, V. G., SKLOVSKAYA, J. S. & SKLOVSKIY, Y. B. 1975 In *Space Studies in the Ukraine*, no. 1 (ed. E. Pisarenko). Kiev: Naukova Domka. Available as *NASA Tech. Transl.* F 15, p. 535.

BIRIKH, R. V. 1966 Thermocapillary convection in a horizontal layer of liquid. *J. Appl. Mech. Tech. Phys.* **3**, 43.

BLOCK, M. J. 1956 Surface tension as the cause of Bénard cells and surface deformation in a liquid film. *Nature* **178**, 650.

BUSSE, F. H. 1972 The oscillatory instability of convection rolls in a low Prandtl number fluid. *J. Fluid Mech.* **52**, 97.

CHANG, CH. E. & WILCOX, W. R. 1976 Analysis of surface tension driven flow in floating zone melting. *Int. J. Heat Mass Transfer* **19**, 355.

CHANG, CH. E., WILCOX, W. R. & LEFEVER, R. A. 1979 Thermocapillary convection in floating zone melting: influence of zone geometry and Prandtl number at zero gravity. *Mat. Res. Bull.* **14**, 527.

CHUN, C.-H. & WUEST, W. 1978 A microgravity simulation of the Marangoni convection. *Acta Astronautica* **5**, 681.

CHUN, C. H. & WUEST, W. 1979 Experiments on the transition from steady to oscillatory Marangoni convection in a floating zone under reduced gravity effect. *Acta Astronautica* **6**, 1073.

CLARK, P. A. & WILCOX, W. R. 1980 Influence of gravity on thermocapillary convection in floating zone melting of silicon. *J. Cryst. Growth* **50**, 461.

CLEVER, R. M. & BUSSE, F. H. 1974 Transition to time dependent convection. *J. Fluid Mech.* **65**, 625.

D'ANS-LAX 1964 *Taschenbuch für Chemiker und Physiker*, vol. II. Springer.

GRODZKA, P. G. & BANNISTER, T. C. 1975 Heat flow and convection experiments aboard Apollo 17. *Science* **187**, 165.

HEYWANG, W. 1956 Zur Stabilität senkrechter Schmelzzonen. *Z. Naturforsch.* **11** A, 238.

JANZ, G. J. 1967 *Molten Salts Handbook*. Academic.

LANDOLT-BÖRNSTEIN 1969 *Zahlenwerte und Funktionen*, vol. 2, part 5A. Springer.

LANDOLT-BÖRNSTEIN 1971 *Zahlenwerte und Funktionen*, vol. 2, part 1. Springer.

LANGLOIS, W. E. 1980 Digital simulation of Czochralski bulk flow in microgravity. *J. Cryst. Growth* **48**, 25.

LANGLOIS, W. E. 1981 Conservative differencing procedures for rotationally symmetric flow with swirl. *Comp. Meth. in Appl. Mech. & Engng* **25**, 315.

LEVICH, B. G. 1962 *Physico-Chemical Hydrodynamics*. Prentice-Hall.

NIELD, D. A. 1964 Surface tension and buoyancy effects in cellular convection. *J. Fluid Mech.* **19**, 341.

OSTRACH, S. 1977 Motion induced by capillarity. In *Proc. Int. Conf. on Physico-Chemical Hydrodynamics* (*Levich Conferenece* 1977). St Peter Port, Guernsey, U.K.: Advance Publications.

PEARSON, J. R. A. 1958 On convection cells induced by surface tension. *J. Fluid. Mech.* **4**, 489.

PREISSER, F. 1981 Die thermische Marangonikonvektion in zylindrischen Schmelzzonen. Thesis, Justus-Liebig-Universität Giessen.

SCHWABE, D. 1981*a* Marangoni effects in crystal growth melts. *Physicochem. Hydrodyn.* **2**, 263.

SCHWABE, D. 1981*b* Marangonikonvektion in Schmelzen. Habilitationsschrift, Justus-Liebig-Universität Giessen.

SCHWABE, D., PREISSER, F. & SCHARMANN, A. 1982 Verification of the oscillatory state of thermocapillary convection in a floating zone under low gravity. *Acta Astronautica* **9** (in the press).

SCHWABE, D. & SCHARMANN, A. 1979 Some evidence for the existence and magnitude of a critical Marangoni number for the onset of oscillatory flow in crystal growth melts. *J. Cryst. Growth* **46**, 125.

SCHWABE, D. & SCHARMANN, A. 1980 Thermocapillary convection in crystal growth melts. *Lett. Heat Mass Transfer* **7**, 283.

SCHWABE, D. & SCHARMANN, A. 1981 Marangoni convection in open boat and crucible. *J. Cryst. Growth* **52**, 435.

SCHWABE, D., SCHARMANN, A. & PREISSER, F. 1979 Steady and oscillatory Marangoni convection in floating zones under 1-*g*. *ESA* SP-142, 327.

SCHWABE, D., SCHARMANN, A. & PREISSER, F. 1980 Konvektion in einer floating zone ohne Rotation. *DGLR-Bericht* 80-02, p. 323.

SCHWABE, D., SCHARMANN, A. & PREISSER, F. 1982 Studies of Marangoni convection in floating zones. *Acta Astronautica* **9**, 183.

SCHWABE, D., SCHARMANN, A., PREISSER, F. & OEDER, R. 1978 Surface tension driven flow in floating zone melting. *J. Cryst. Growth* **43**, 305.

SCRIVEN, L. E. & STERNLING, C. V. 1964 On cellular convection driven by surface-tension gradients: effects of mean surface tension and surface viscosity. *J. Fluid Mech.* **19**, 321.

SMITH, K. A. 1966 On convection instability induced by surface-tension gradients. *J. Fluid Mech.* **24**, 401.

SMITH, M. K. & DAVIS, S. H. 1981 Instability of a thermocapillary shear flow. *European Mechanics Colloquium* 138, *Karlsruhe*, 9–11 *March*, 1981, *abstracts* pp. 129–130.

WILLIS, G. E. & DEARDORFF, J. W. 1970 The oscillatory motions of Rayleigh convection. *J. Fluid Mech.* **44**, 661.